Highly Efficient and Robust Blue Phosphorescent Pt(II) Compounds with a Phenyl-1,2,3-triazolyl and a Pyridyl-1,2,4-triazolyl Chelate Core

*Xiang Wang, Shao-Long Gong, Datong Song, Zheng-Hong Lu, and Suning Wang**

A new class of brightly phosphorescent Pt(II) compounds that contain an N^C-chelate phenyl-1,2,3-triazolyl ligand (ptrz) and an N^C-chelate pyridyl-1,2,4-triazolyl ligand (pytrz) in the central core is achieved. The impact of various substituent groups on phosphorescence of this class of molecules is examined. Crystal structural analyses revealed that this class of compounds has a great tendency to form stacked dimers—one of which is persistent even in the gas phase—leading to excimer emission. The introduction of bulky substituents, such as diphenyl amino (NPh_2) or trityl (CPh_3), is found to greatly diminish the excimer emission. Using this approach, several highly efficient blue and green phosphorescent Pt(II) compounds with λ_{em} at ≈450–460 nm and $\Phi_p \approx 0.70$ to 1.00 are obtained. These molecules are highly robust with exceptionally high thermal stability. Bright bluish-green electrophosphorescent devices with external quantum efficiencies as high as 16.7% are fabricated.

1. Introduction

A key challenge in the research and development of organic light emitting diodes (OLEDs) is efficient and stable triplet blue emitters.[1] Much current research efforts on blue triplet emitters focus on Ir(III)-based systems.[2] Although many highly efficient blue phosphorescent Ir(III) compounds have been reported in the literature,[3] they are still not satisfactory for practical use in OLEDs because of their poor stability in OLEDs. As a class of alternative triplet blue emitters, Pt(II)-based systems have gained much recent research interest,[4] although efficient blue phosphorescent Pt(II) compounds remain rare.[5] The large ligand field splitting energy in square planar Pt(II) compounds is advantageous to access efficient blue emitters because of the reduced probability of thermal quenching via the metal-centered d-d states.[6] On the other hand, the flat structure of Pt(II) compounds makes them highly prone to excimer formation and distortion in the excited state, causing the shift of the emission color toward longer wavelengths, typically yellow or orange and a significant reduction of emission quantum efficiency.[7] Thus, increasing the steric bulk around the Pt(II) unit is a key strategy to enhance the phosphorescent emission quantum efficiency in Pt(II)-based systems, which has been successfully demonstrated by a number of research teams.[8] We have recently shown that a dimesitylboryl unit ($BMes_2$) is highly effective in enhancing the phosphorescent and electrophosphorescent efficiency of N^C- or C^C-chelated Pt(II) compounds.[9] The role of the $BMes_2$ unit was found to be multitude, including facilitating metal-to-ligand charge transfer (MLCT) and electron transporting process in OLEDs.[8d] Another important role of the $BMes_2$ unit is to provide steric shielding to the Pt(II) unit, owing to its large size, that greatly reduces the formation of excimer emission. Using this approach, we have successfully developed a series of blue and blue-green phosphorescent Pt(II) compounds and demonstrated their use in OLEDs.[8d,9] The best blue emitters based on $BMes_2$-functionalized Pt(II) compounds are shown in **Scheme 1** that contain a *m*-$BMes_2$-phenyl-1,2,3-triazolyl (*m*-Bptrz) chelate as the chromophore and a pyridyl-1,2,4-triazolyl (pytrz) chelate as the ancillary ligand.[9e] Although these molecules display a high phosphorescent quantum efficiency (Φ_P) in films (e.g., PMMA) at a low doping concentration, the excimer formation became significant, accompanied by a substantial decrease of Φ_P at higher doping concentrations (e.g., R_1 = Me, R_2 = ^{t}Bu, Φ_P = 0.97 in 5 wt% of PMMA, 0.65 in 10 wt% of PMMA; R_1 = Me, R_2 = CF_3, Φ_P = 0.71 in 5 wt% of PMMA, 0.47 in 10 wt% of PMMA), which became much more pronounced in OLEDs.[9e] This is caused mainly by the propensity of the triazolyl unit to stack and the *meta*-location of the $BMes_2$ group that is not completely effective in shielding the central core from excimer formation. Moving the $BMes_2$ unit to the *para*-position for more effective steric shielding is not an option since it shifts

X. Wang, Prof. S. Wang
Department of Chemistry
Queen's University
Kingston, Ontario K7L 3N6, Canada
E-mail: wangs@chem.queensu.ca
Dr. S.-L. Gong, Prof. Z. H. Lu
Department of Materials Science and Engineering
University of Toronto
Toronto, Ontario M5S 3E4, Canada
Prof. D. T. Song
Department of Chemistry
University of Toronto
80 St George St., Toronto, Ontario M5S 3H6, Canada

DOI: 10.1002/adfm.201402366

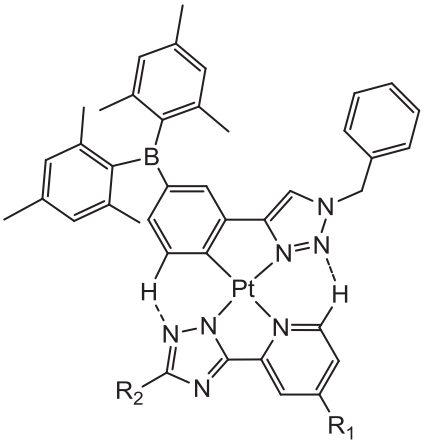

(*m*-L1)Pt(R_2-pytrz-R_1)

R_1 = H or Me; R_2 = H or ^{t}Bu, or CF_3

Scheme 1. The structure of m-BMes2-functionalized Pt(II) compounds.

the emission energy to green.[9] Nonetheless, our prior study on the *m*-$BMes_2$ functionalized Pt(II) compounds revealed that the Pt(II) unit with the *m*-Bptrz and the pytrz chelate ligands have interesting features. For example, there are two intramolecular hydrogen bonds in the central core, which could minimize the structural distortion of the molecule in the excited state. Furthermore, computational studies suggested that the central core of this class of molecules has a triplet energy in the blue region, making them attractive for further investigation as potential blue emitters for OLEDs. One weakness of $BMes_2$-functionalized Pt(II) compounds is that they have a relatively low thermal stability (typically less than 250 °C), which could have a negative impact on their vacuum deposition and their performance in OLEDs. Thus, with the aim to develop a new class of highly robust blue phosphorescent Pt(II) compounds that are relatively easy to access synthetically, we carried out the investigation on new Pt(II) compounds based on the ptrz (phenyl-1,2,3-triazolyl) and the pytrz central core, which lack the $BMes_2$ unit. The key approach we employed is to provide steric shielding for the central Pt(II) unit using non-borylated groups. Highly efficient blue, blue-green and green Pt(II) phosphorescent emitters with a high thermal stability have been achieved and their performance in OLEDs has been evaluated. The details are presented herein.

2. Results and Discussion

2.1. Syntheses

Five ptrz derivative ligands **L1**–**L5** were selected and synthesized as the N^C-chelate chromophores for the Pt(II) compounds. The 1,2,3-triazolyl portion of ligands **L1**–**L4** contains a benzyl group while that in **L5** has a diphenylmethyl group. **L1** has no substituent on the phenyl portion of the chelate while **L2** and **L3** have two fluorine atoms and a diphenylamino group on the phenyl ring, respectively, which were intended to alter the HOMO–LUMO gap in order to tune the emission color of the corresponding Pt(II) complexes. For **L3**, the bulky NPh_2 group also provides steric shielding to the Pt(II) unit to minimize excimer emission. **L4** and **L5** contain a trityl (CPh_3) group at the *para*-position of the phenyl ring which was intended to increase the steric bulk around the Pt(II) unit while decreasing the electron donation to the chelate core. **L1** and **L2** were synthesized using a modified procedure from literature,[10] which involves the reaction of phenylacetylene or 1-ethynyl-2,4-difluorobenzene with benzyl azide in water and the presence of copper iodide in a sealed tube at 50 °C overnight. This procedure works the best for starting materials that are either liquid or have low melting points because after the reaction is finished, the product simply precipitates out and can be purified by just filtering and washing. **L3** – **L5** were synthesized using the procedure similar to that[9e] employed for *m*-Bptrz ligands we reported earlier (**Scheme 2**). This procedure gives higher yields (≈70%), compared to the first one (≈50%), but aqueous work up and column chromatography are needed to obtain the purified product. Ligand **L3**, **L4** and **L5** are new compounds and characterized by NMR spectroscopic analyses. Two Me-pyridyl-1,2,4-triazole ancillary ligands (Me-pytrz) were synthesized by previously published procedures.[2d,11] The ^{t}Bu and the CF_3 subtituents on the Me-pytrz ligand allowed us to examine the steric and electronic impact of the ancillary ligand on the phosphorescence of the Pt(II) compounds.

Nine Pt(II) compounds with different combinations of the chelate chromophore ligands and the ancillary ligands were synthesized using a modified one-pot procedure developed by our group (**Scheme 3**).[12] The appropriate ptrz ligand and $[PtMe_2(SMe_2)]_2$ were heated at 70 °C for 1 h in acetone, followed by the addition of tosylic acid (TsOH) and the subsequent addition of the corresponding Me-pytrz ancillary ligand. After

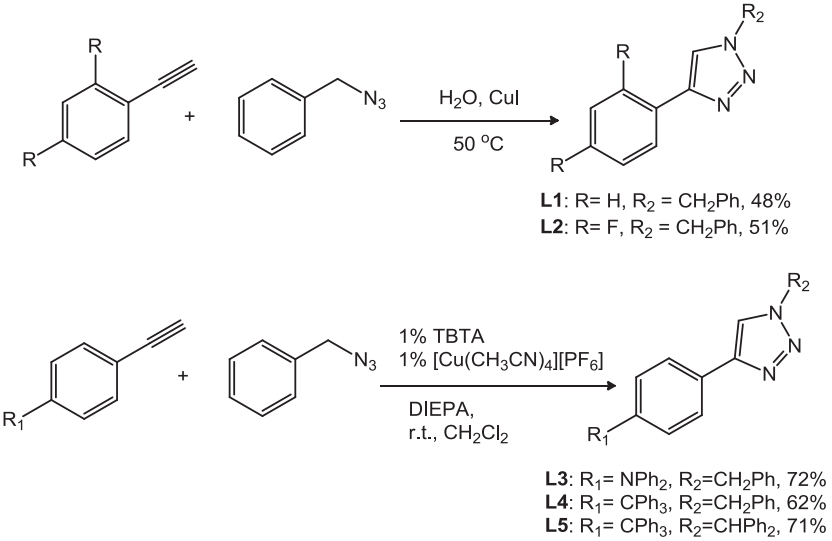

Scheme 2. The syntheses of ligands.

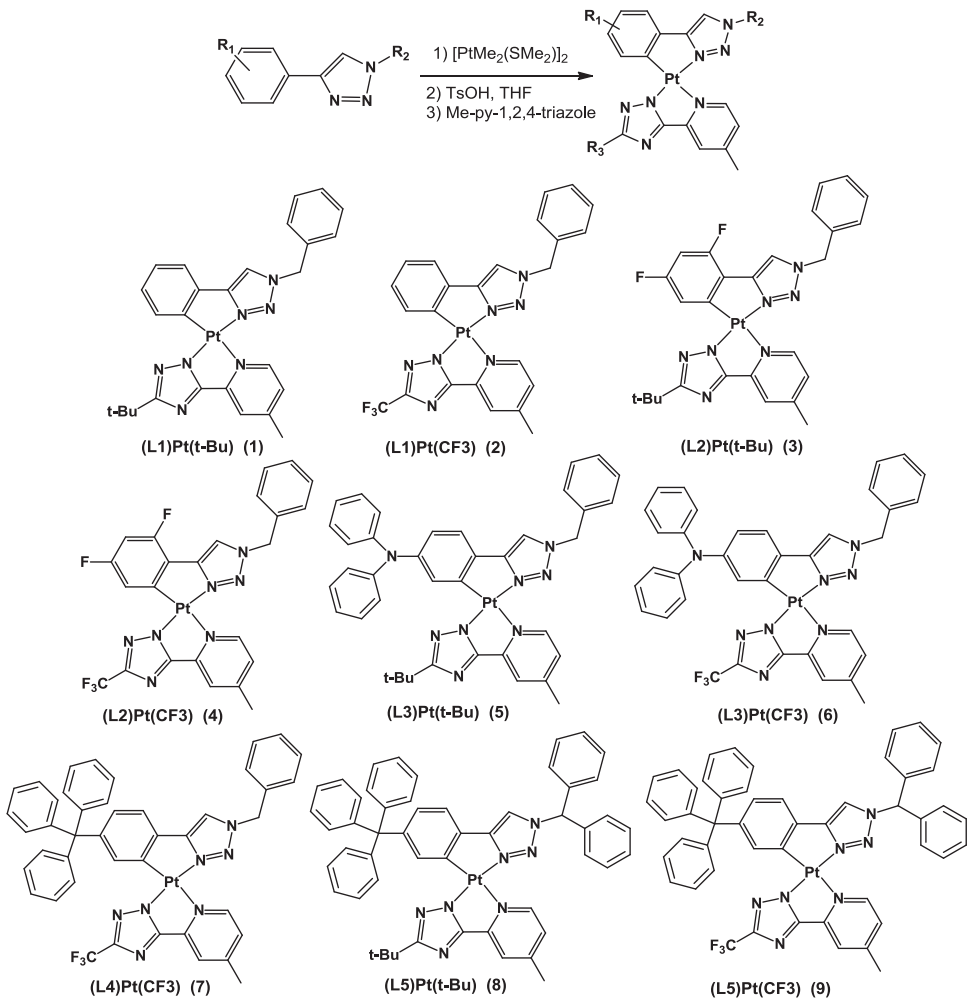

Scheme 3. The syntheses and structures of Pt(II) compounds.

purification, the Pt(II) compounds were obtained in 14–46% yields. All Pt(II) compounds have been fully characterized by NMR and elemental analyses.

2.2. Crystal Structures of Pt(II) Compounds

The crystal structures of compounds **4**, **5**, **7**, **8** and **9** have been determined by single-crystal X-ray diffraction analyses. Important bond lengths and angles of these compounds are given in **Table 1**. As shown in **Figure 1**, the molecules of **4** form a stacked dimer with a very short Pt···Pt separation distance (3.228(1) Å).[13] The pytrz chelate ligand stacks with the ptrz ligand with short separation distances (3.35 – 3.50 Å). Between the dimers, the Pt···Pt separation distance is much larger (5.238(1) Å). Compound **4** exists also likely as a dimer in solution as evidenced by the distinct downfield shift (~0.50 ppm) of the two singlet peaks in the ^{1}H NMR spectrum of **4**, compared to those of **3** (see **Scheme 4** and SI). Mass spectroscopic analysis further revealed that **4** exists as a dimer in the gas phase. DFT computational data indicated that the HOMO and LUMO of **4** are localized mainly on the ptrz-Pt and the py-trz chelate unit, respectively (see the computational section below), which clearly favors intermolecular π-stacking between these two units. The attractive Pt···Pt interaction and the flat structure of **4** further reinforce the dimer formation. Although discrete dimers were not observed for compound **3** in MS spectroscopic analysis, intermolecular π-stacking interactions are possible for this molecule, owing to its flat and open structure.

The crystal structures of **5** and **7** are shown in **Figure 2** while those of **8** and **9** in **Figure 3**. In contrast to compound **4**, no significant intermolecular interactions were observed in the crystal lattice of **5** with the shortest Pt···Pt separation distance being 6.508(1) Å. The bulky NPh_2 group along with the *t*-Bu group is clearly effective in preventing intermolecular stacking. Interestingly, despite the presence of the bulky CPh_3 group in **7**, extended and partial π stacking were observed in the crystal lattice of **7**, as shown in **Figure 4**. The Pt···Pt separation distances are 4.819(1) Å and 5.850(1) Å, respectively between the neighboring molecules, and the shortest atomic separation distance is ≈3.5 Å between the heterocyclic chelate ligands in **7**. This indicates that the CF_3 on the ancillary ligand is not very effective in blocking intermolecular interactions. This is further supported by the crystal structure of **9**, in which the

Table 1. Important bond lengths (Å) and angles (°) of the Pt(II) compounds.

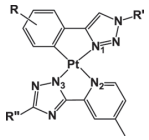

	Pt-C	Pt-N_1	Pt-N_2	Pt-N_3	Pt···Pt	N_2-Pt-C / N_1-Pt-N_3
(L2)Pt(CF_3) (**4**)	2.024(9)	2.007(7)	2.120(8)	1.981(7)	3.2276(4)	175.8(3)/ 176.9(3)
	2.012(9)	1.974(7)	2.117(8)	1.979(8)		179.3(3)/ 177.3(3)
(L3)Pt(CF_3) (**5**)	1.978(8)	2.003(7)	2.133(7)	1.979(7)	6.508(1)	177.0(2)/178.3(3)
(L4)Pt(CF_3) (**7**)	1.995(9)	1.979(8)	2.124(7)	1.991(8)	4.819(1)	178.8(3)/179.5(3)
(L5)Pt(t-Bu) (**8**)	2.017(3)	2.004(3)	2.133(3)	1.985(3)	4.960(1)	178.14(15)/179.23(12)
(L5)Pt(CF_3) (**9**)	1.980(11)	2.001(7)	2.098(9)	2.002(7)	4.294(1)	178.4(3)/179.4(3)

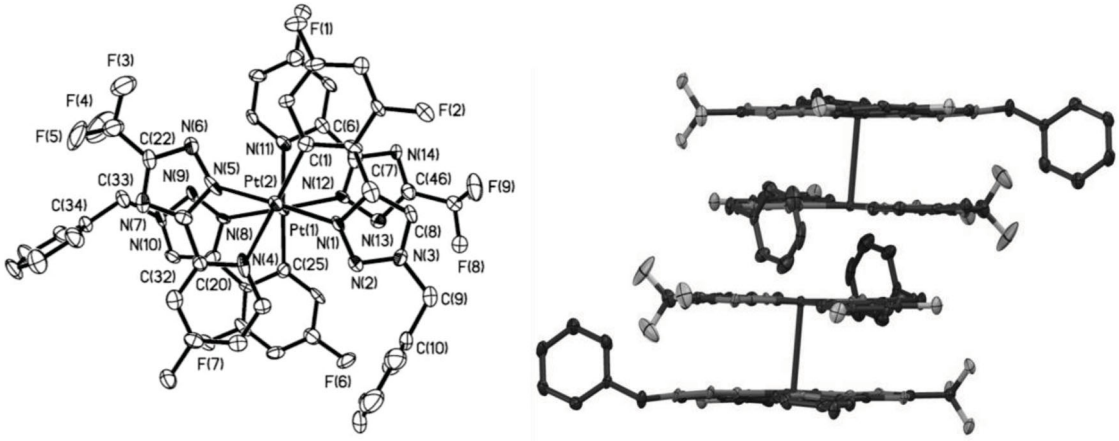

Figure 1. The crystal structure of compound **4**, showing the stacked dimer (left: top view, right: side view), with labeling schemes and 50% thermal ellipsoids. H atoms are omitted for clarity.

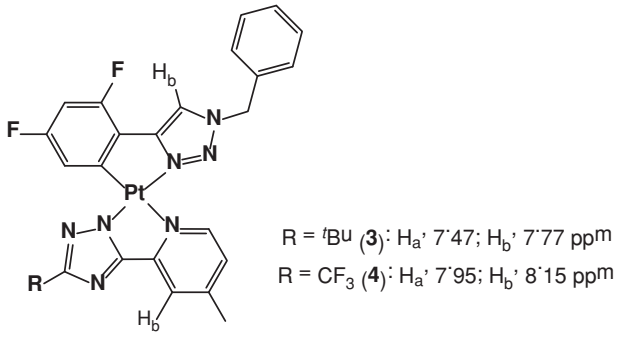

Scheme 4. The structures of compounds 3 and 4 and the chemical shifts of Ha and Hb.

benzyl group is replaced by a diphenylmethyl group but the molecule still forms partially π-stacked dimers in the crystal lattice, as shown in Figure 6, with a Pt···Pt separation distance of 4.294(1) Å. The *t*-Bu group in **8** appears to be more effective in minimizing π-stacking interactions, as evidenced by the longer Pt···Pt separation distance of 4.960(1) Å within the partially π-stacked dimer of **8** and the lack of extended π-stacking interactions (Figure 4).

The crystal structural data show that the introduction of a bulky substituent group such as NPh_2 or CPh_3 on the ptrz chelate ligand is indeed effective in substantially reducing π-stacking and Pt···Pt interactions. For the pytrz chelate ligand, a *t*-Bu group is more effective than a CF_3 group in reducing intermolecular interactions among the Pt(II) molecules.

2.3. Thermal Stability

To examine the thermal stability of the new class of Pt(II) compounds and compare them with the $BMes_2$-functionalized compounds, thermogravimetric analysis (TGA) was performed for vacuum dried samples of compounds **7**–**9** and ($BMes_2$)-**7** (R_1 = Me, R_2 = *t*-Bu in Chart 1). All four compounds contain solvent molecules in their crystal lattices, according to the X-ray crystal structural data (1 THF for **7**; 2, 2.4 and 1 CH_2Cl_2 for **8**, **9**, and ($BMes_2$)-**7**, respectively). To remove these solvent molecules, all samples were kept under vacuum over night and heated for 10 min at 100 °C under nitrogen before the TGA diagrams were recorded. As shown by the TGA diagrams recorded under nitrogen atmosphere in **Figure 5**, it is evident that the

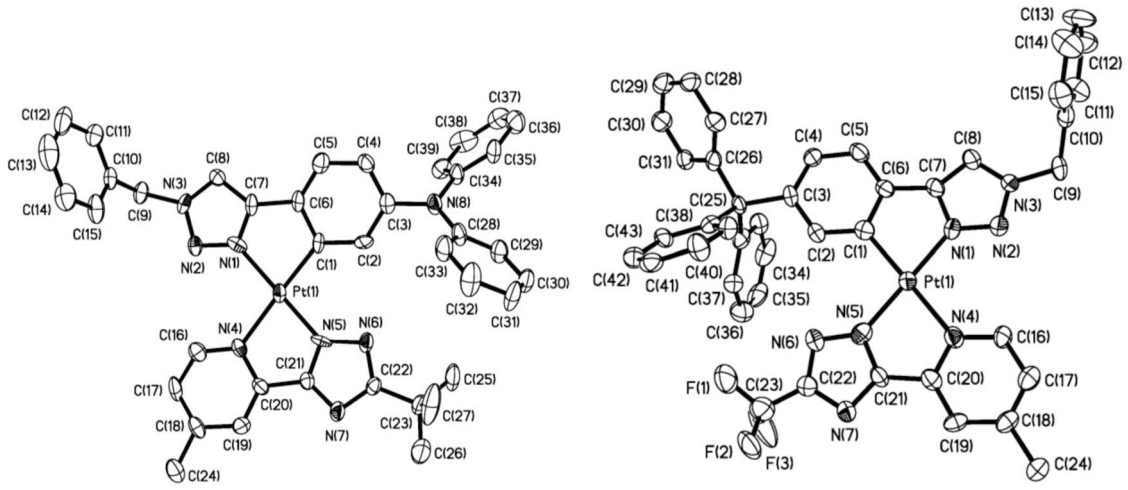

Figure 2. The crystal structures of compound **5** (left) and **7** (right) with labeling schemes and 50% thermal ellipsoids. H atoms are omitted for clarity.

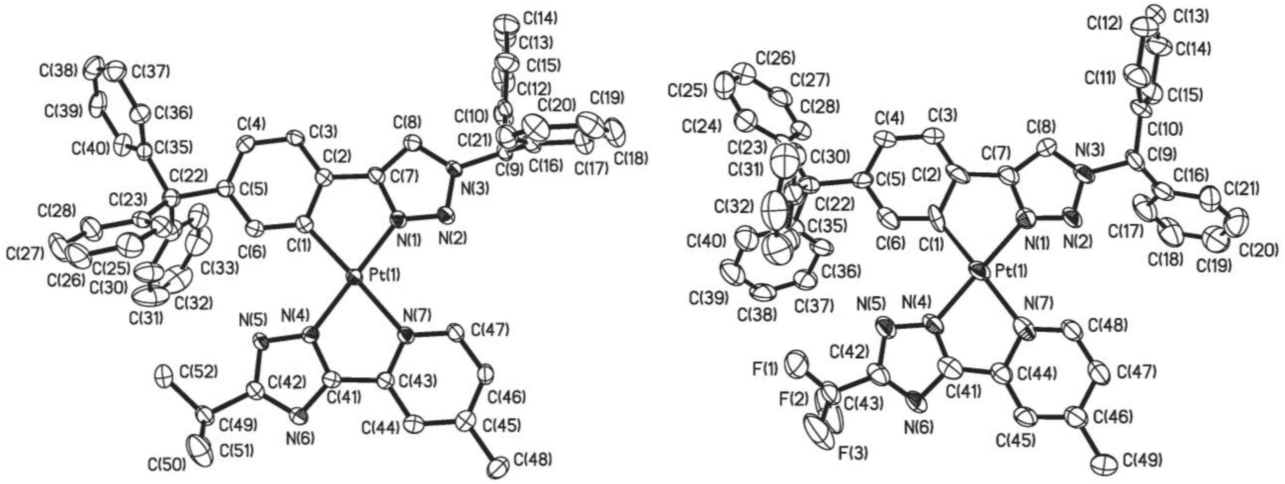

Figure 3. The crystal structures of compound **8** (left) and **9** (right) with labeling schemes and 50% thermal ellipsoids. H atoms are omitted for clarity.

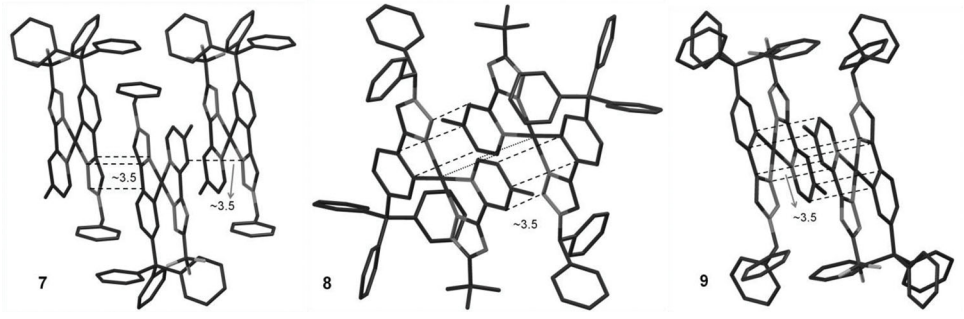

Figure 4. A diagram showing intermolecular π stacking interactions in the crystal lattice of **7**, **8**, and **9**.

$BMes_2$-functionalized molecule is the least stable thermally while compound **7** is the most stable and does not show any weight loss until ≈400 °C. Compounds **8** and **9** also display an excellent thermal stability up to ~350°C. The less than 2% weight loss of **8** below 350 °C is likely caused by the loss of residual solvent molecules. These data confirmed the relatively low thermal stability of $BMes_2$-functionalized compounds (most likely the dissociation of the $BMes_2$ unit from the chelate ligand, corresponding to ≈28% weight loss) and the robustness of the non-$BMes_2$ functionalized Pt(II) molecules.

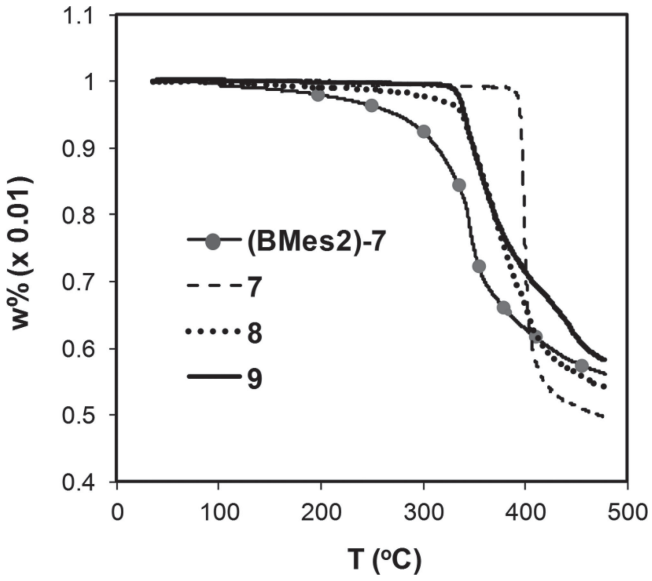

Figure 5. TGA diagrams for compounds **7**–**9** and ($BMes_2$)-**7**, recorded under nitrogen.

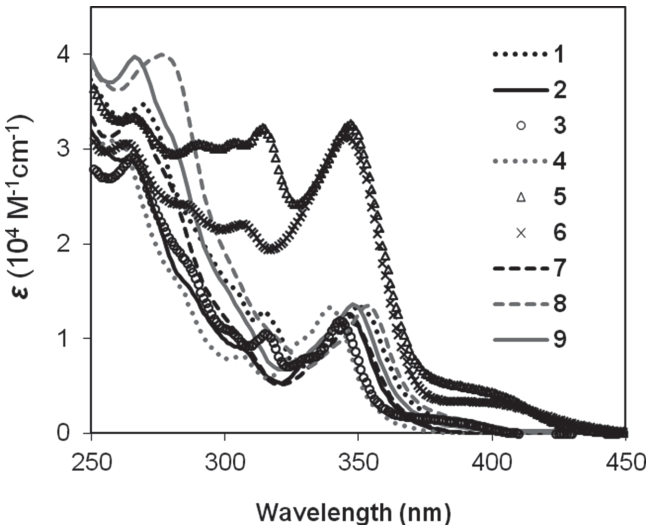

Figure 6. Absorption spectra of compounds **1**–**9** in CH_2Cl_2 at ambient temperature.

2.4. Photophysical Properties

The photophysical properties of the Pt(II) compounds are summarized in **Table 2**. As shown in **Figure 6**, all complexes show strong absorption bands at around 350 nm (ε = 13 000–30 000 M^{-1} cm^{-1}), which could be attributed to ligand centered transitions. Compared to the $BMes_2$-functionalized Pt(II) compounds with a similar central core,[9e] the energy of this absorption band is blue shifted by ≈10 nm and is less intense, except for compounds **5** and **6**, which have much larger extinction coefficients (≈30 000 M^{-1} cm^{-1}), attributable to an intramolecular charge transfer transition involving the electron rich diphenylamino group. Compounds **5** and **6** also display a distinct MLCT band at ≈400 nm that is much more intense than those in other compounds.

Compounds **1**–**9** display weak to moderate phosphorescence with Φ_p up to 0.30 in deaerated CH_2Cl_2 at ambient temperature. The decay lifetimes of all compounds in frozen CH_2Cl_2 glass are in the microsecond range, indicating that the nature of the luminescence is phosphorescence. However, all complexes show much brighter emission in frozen glass (see SI), as neat solid or in 5% or 10% doped PMMA films (**Figure 7**), with the emission color ranging from blue to yellow or white. The electronic properties and the steric bulkiness of the substituent group have been found to play very important roles in the emission color and the Φ_p of this class of compounds, which will be discussed in details below.

Table 2. Photophysical data of Compounds **1**–**9**.

Compound	Absorption[a] λ_{max} [nm] ε [10^4 $cm^{-1}M^{-1}$]	Emission, λ_{max} [nm], 298 K						Emission 77 K[c]	
		λ_{max} [nm]			Φ_{PL}[b]			λ_{max} [nm]	τ_P [μs]
		CH_2Cl_2	PMMA [wt%]		CH_2Cl_2	PMMA [wt%]			
			5%	10%		5%	10%		
(L1)Pt(t-Bu) (**1**)	315 (1.30), 350 (1.37)	510	465,497	465,499	0.06	0.84	0.96	470	7.3
(L1)Pt(CF_3) (**2**)	305 (0.91), 344 (1.24)	–	552	553	<0.001	0.64	0.29	440/556	4.2/–
(L2)Pt(t-Bu) (**3**)	315 (1.05), 343 (1.19)	509	500	543	0.25	0.79	1.00	466/ 501	–/8.7
(L2)Pt(CF_3) (**4**)	303 (0.79), 338 (1.31)	564	595	610	0.01	0.27	0.15	440/ 535	–/5.7
(L3)Pt(t-Bu) (**5**)	314 (3.23), 345 (3.24)	514	486	491	0.21	0.92	0.59	494	23.9
(L3)Pt(CF_3) (**6**)	302 (2.17), 344 (3.12)	542	500	510	0.30	1.00	1.00	501/ 543	17.6/13.1
(L4)Pt(CF_3) (**7**)	264 (3.34), 348 (1.16)	–	454	455	<0.001	1.00	0.89	448/ 543	7.7/ 3.6
(L5)Pt(t-Bu) (**8**)	276 (4.00), 354 (1.35)	512	468496	468498	0.13	0.90	0.95	460	5.3
(L5)Pt(CF_3) (**9**)	266 (3.98), 348 (1.36)	–	452	453	<0.001	0.68	0.72	448	7.8

[a]Measured in CH_2Cl_2 at 2×10^{-5} M; [b]The solution quantum efficiency was determined in CH_2Cl_2 using $Ir(ppy)_3$ as the reference under nitrogen. The solid state quantum efficiency was measured using an integration sphere. All quantum yields are ± 10%; [c]Recorded in CH_2Cl_2 (≈2.0×10^{-5} M).

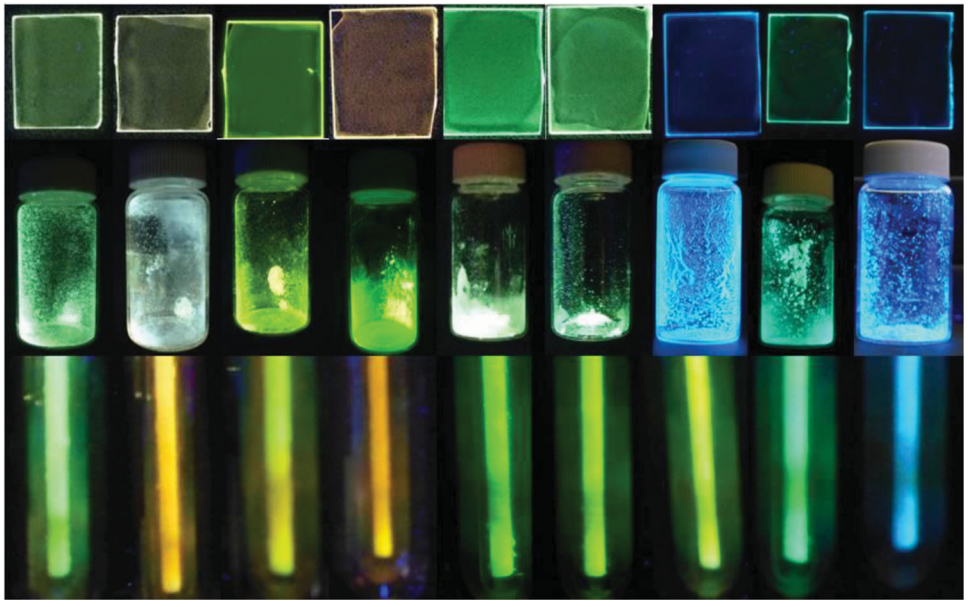

Figure 7. Photographs showing the emission colors of compounds **1**–**9** in 5 wt% PMMA films (top), as neat solids (middle) and in frozen CH_2Cl_2 glass (≈2.0×10^{-5} M, bottom) at 77 K.

2.4.1 Compounds 1 and 2: the t-Bu and the CF_3 Substituent Effect

The phosphorescent spectra of compounds **1** and **2** (**Figure 8**), which contain an unsubstituted phenyl ring in the ptrz ligand, display well resolved vibronic features in frozen CH_2Cl_2 at 77 K, an indication that the emission is originated from an admixture of ^{3}LC and ^{1}MLCT states. The λ_{max} of the emission spectra of **1** and **2** at 77 K is at 470 and 440 nm, respectively, supporting that the substituent on the Me-pytrz ligand has a significant contribution to the phosphorescence since there is a 30 nm difference in emission energy between these two molecules. A broad and featureless band at 556 nm was observed in the emission spectrum of **2** at 77 K, which is from the excimer emission and accounts for the yellow emission color of **2**. In contrast, no significant excimer emission was observed for **1** at 77 K. In the doped PMMA films, the emission of **2** displays nearly a pure excimer emission (λ_{max} ≈ 550 nm) with a white and a yellow emission color at 5 wt% and 10 wt% doping level, respectively, while that of **1** resembles the spectrum at 77 K albeit more broad with a greenish blue color. The persistent excimer emission of **2** is in agreement with our previous observation that compounds with a CF_3 group on the pytrz ligand are more prone to excimer formation than those with a t-Bu group.[9e] Compound **2** shows a stronger tendency for excimer emission compared to its *meta*-borylated counterpart (*m*-L1)Pt(CF_3-pytrz-Me) owing to the lack of a bulky $BMes_2$ group. It is noteworthy that the λ_{max} of **2** at 77 K is blue shifted by ≈15 nm compared to that of (*m*-L1)Pt(CF_3-pytrz-Me), indicating the potential to obtain deep blue phosphorescence using the same central core unit. Compound **1** has a very impres-

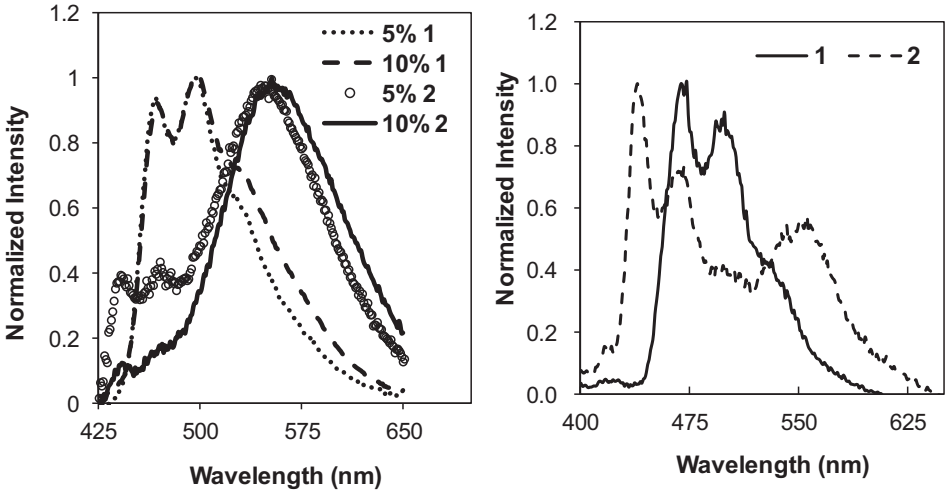

Figure 8. The phosphorescent spectra of **1** and **2** in PMMA at ambient temperature (left) and in frozen CH_2Cl_2 solution at 77 K (right).

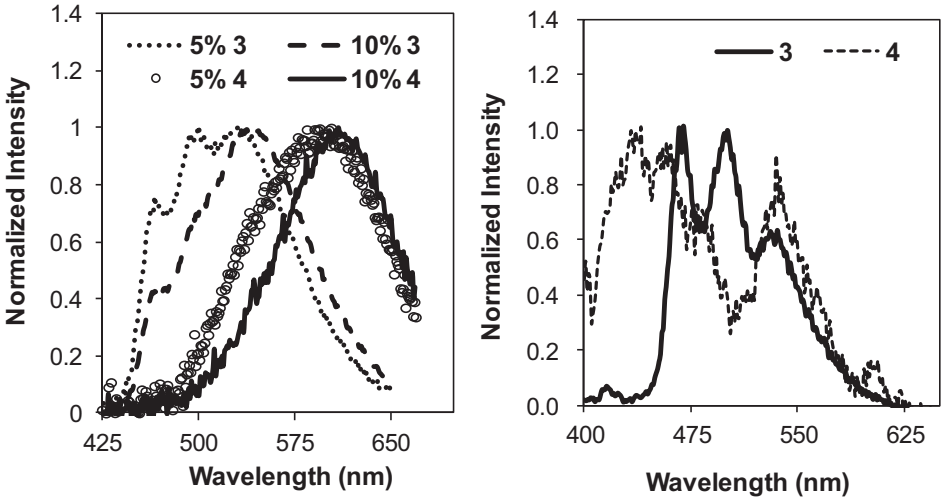

Figure 9. The phosphorescent spectra of **3** and **4** in PMMA at ambient temperature (left) and in frozen CH_2Cl_2 solution at 77 K (right).

sive high Φ_p in the solid state (0.84 in 5 wt% PMMA, 0.96 in 10 wt% PMMA), which are comparable to the *meta*-borylated counterpart (*m*-L1)Pt(t-Bu-pytrz-Me) (0.97 in 5 wt% PMMA, 0.65 in 10 wt% PMMA).[9e]

2.4.2. Compounds 3 and 4: the Fluorine Substitution Effect

A commonly used approach to tune the emission color of the cyclometallated Pt(II) complexes is to manipulate their HOMO or LUMO levels by introducing different functional groups. Thompson and co-workers observed a 20 nm blue-shift in the emission energy when the 4′ and 6′ positions of the phenyl ring in Pt(ppy)(acac) are substituted by two fluorine atoms.[4a] We thus tried the same approach by introducing two fluorine atoms on the ptrz ligand in molecules **3** and **4**. As shown in **Figure 9**, the λ_{em} of **3** at 77 K is about 5 nm blue shifted, relative to that of **1**, while those of **2** and **4** are similar with a similar excimer peak at 77 K. At ambient temperature, in PMMA films, the phosphorescent spectrum of **4** is a pure excimer emission at a 5 wt% and a 10 wt% doping level with a low Φ_P (0.27 and 0.15, respectively), while that of **3** has a significant excimer contribution at both the 5 wt% and 10 wt% doping levels, although the Φ_P of **3** is still impressive (0.79 in 5 wt% PMMA, 1.00 in 10 wt% PMMA). These data indicate that the incorporation of fluorine atoms in the ptrz based system greatly enhances the excimer formation. The unusually high tendency for compound **4** to produce emcimer emission can be rationalized by the formation of intrinsic dimers observed by both X-ray crystallography and the mass spectrometry analysis.

2.4.3. Compounds 5 and 6: the NPh_2 Substitution Effect

The diphenyl amino substituted compounds **5** and **6** show green emission in doped PMMA films, in frozen CH_2Cl_2 glass or in CH_2Cl_2 at ambient temperature. The most significant difference between the emission spectra of **5** and **6**, and those of **1**–**4** is that the excimer emission is much less in **5** and **6** in PMMA films at ambient temperature as shown in **Figure 10**. The monomer emission peak of **5** and **6** as revealed by the spectra in frozen CH_2Cl_2 at 77 K is red shifted by about 20 nm and 60 nm, respectively, relative to that of **1** and **2**, which is clearly caused by the electron-donating amino group that raises the HOMO energy, thus decreasing the emission energy. An interesting observation was that the monomer emission energy of **5** and **6** is similar, in contrast to the previous pairs, in which the monomer emission peak of the CF_3 substituted molecule is always at a higher energy than the t-Bu substituted one. This indicates that the phosphorescence of **5** and **6** is most likely from electronic transitions localized on the NPh_2-ptrz chelate. The excimer emission peak of **6** was observed in the 77 K emission spectrum shown in Figure 10 that appears at ~543 nm, similar to those observed for **2** and **4**.

The greatly reduced excimer emission for this pair is in agreement with our previous finding that intermolecular interactions can be effectively suppressed when a bulky group is introduced at the 4′ position of the phenyl ring. The decay lifetimes of **5** and **6** are substantially longer (23.9 μs for **5**, 17.6 μs for **6**) than the other complexes, indicating a larger ^{3}LC contribution in the excited state,[8d] which is likely facilitated by the CT transition from the amino group to the ptrz chelate ring. Both **5** and **6** show excellent quantum yields in doped PMMA films (0.92/0.59 for **5** in 5 wt%/10 wt% PMMA, 1.00 for **6** in both 5 wt% and 10 wt% PMMA), making them good candidates as dopants for green OLEDs.

2.4.4. Compounds 7–9 : the Trityl Substitution Effect

The phosphorescent data of compounds **1**–**6** illustrate that in order to achieve blue phosphorescence using the ptrz based Pt(II) compounds, it is necessary to introduce a bulky substituent at the *para*-position to minimize the excimer emission. In addition, it is necessary to avoid the use of electron donor groups such as amino to minimize the spectral red shift. Therefore, a trityl group was installed at the *para*-position of the ptrz chelae in compounds **7**–**9**.

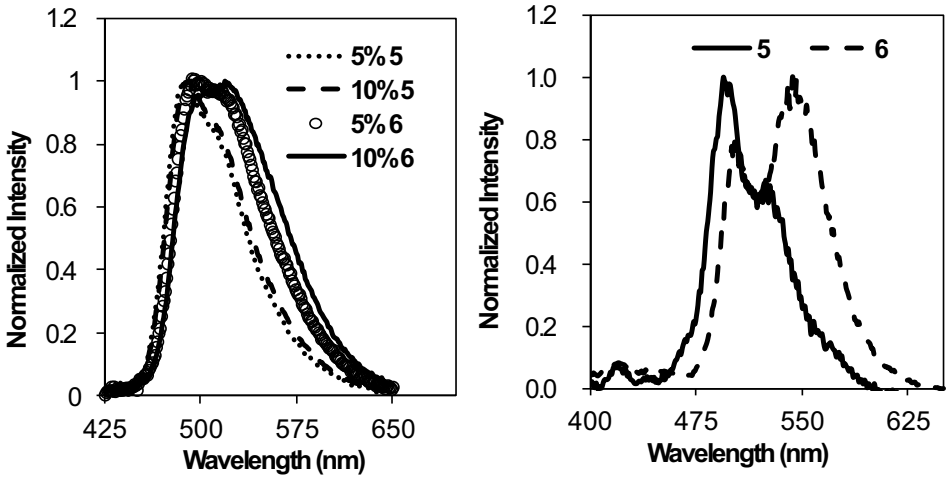

Figure 10. The phosphorescent spectra of **5** and **6** in PMMA at ambient temperature (left) and in frozen CH_2Cl_2 solution at 77 K (right).

As shown in **Figure 11**, no apparent excimer emission was observed in the phosphorescent spectra of compounds **7–9** in PMMA films at the 5 wt% and 10 wt% doping levels, an indication that the incorporation of the trityl group is effective in preventing excimer emission. Most exciting is that the emission maximum of all three compounds lies in the blue region (454 nm for **7**, 468 nm and 496 nm for **8**, and 452 nm for **9**) with excellent quantum efficiencies (1.00/0.89 for **7**, 0.90/0.95 for **8** and 0.68/0.72 for **9**, at the 5 wt% and 10 wt% doping level in PMMA, respectively). The emission energy of **7–9** is in fact similar to the *meta*-borylated analogues,[9e] illustrating the effectiveness of achieving bright blue phosphorescence using a bulky but non-boryl substituent at the *para*-position of the ptrz ligand. The 77 K emission spectra of **7–9** in frozen CH_2Cl_2 match well with those in PMMA at ambient temperature except that of **7** that displays a distinct excimer peak at 543 nm in the 77 K spectrum. This suggests that the diphenylmethyl group in **9** is more effective than the benzyl group in **7** in shielding the molecule from excimer formation. The excimer emission peak of **7** has a much shorter decay lifetime (3.6 μs) than that of the monomer (7.7 μs). The decay lifetimes of the monomer emission of **7–9** are similar to those of the monomer emission peak of **1** and **2** (see Table 2).

2.5. Computational Study

TD-DFT calculations were performed for compounds **1–9** using Gaussian 09 software at B3LYP level of theory using LAN2DZ basis set for Pt atom and 6–31G* for all other atoms.[14] The HOMO-LUMO diagrams for **1**, **2**, **5**, **6**, **8**, and **9** are shown in **Figure 12** while those of **3**, **4** and **7** resemble those of **1**, **2** and **9**, respectively, thus provided in the SI. The Pt d orbital has a large contribution to the HOMO level of all complexes except for compounds **5** and **6**, in which the HOMO involves mainly the phenyl ring and the diphenyl amine group of the ptrz chelate, which is not surprising as the electron donating group significantly raises or destabilizes the HOMO level. For compounds with the CF_3-pytrz ligand, the HOMO is mostly delocalized on the ptrz chelate while for compounds with the *t*-Bu group

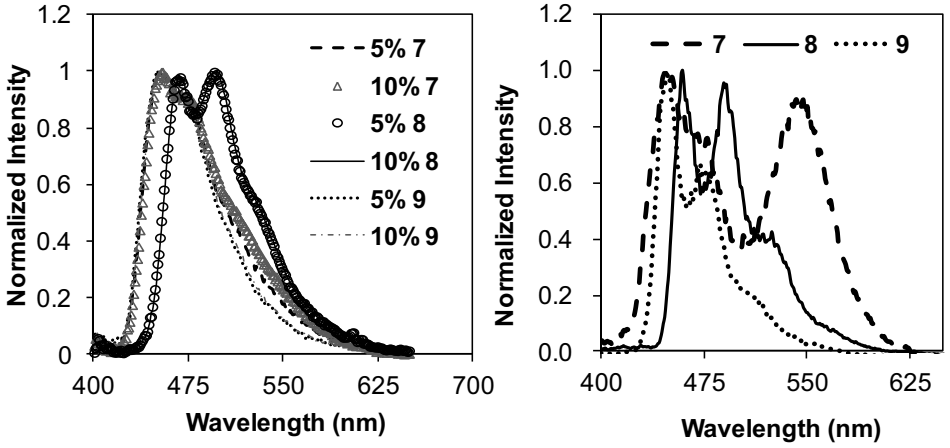

Figure 11. The phosphorescent spectra of **7–9** in PMMA at ambient temperature (left) and in frozen CH_2Cl_2 solution at 77 K (right).

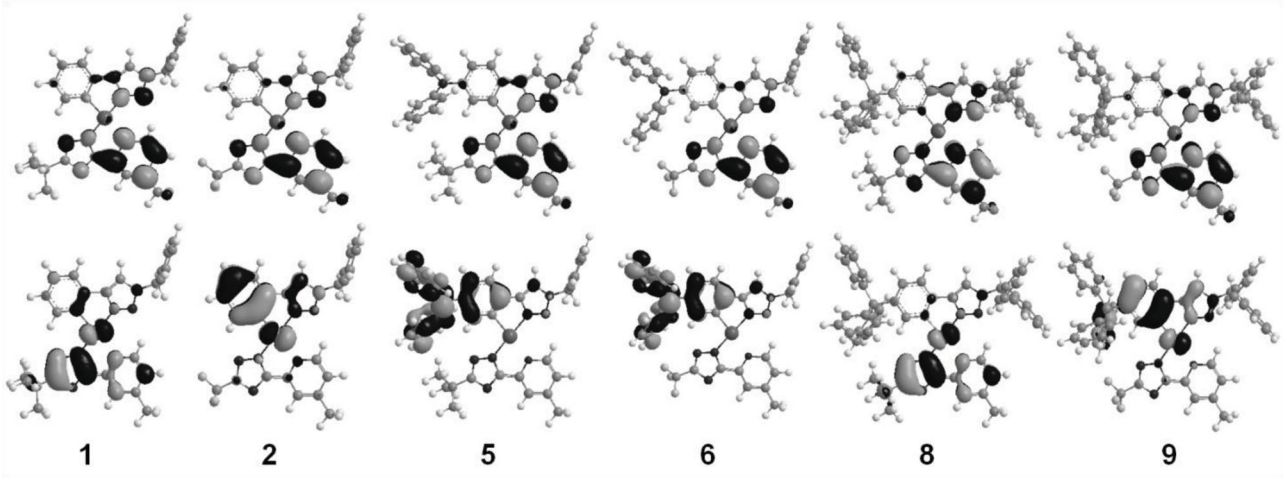

Figure 12. HOMO and LUMO diagrams of selected compounds (isocontour value = 0.03).

the HOMO is mostly located on the pytrz chelate. The fluorine atoms on ptrz and the CF_3 group on pytrz stabilize the HOMO energy substantially, relative to the non-substituted ptrz or the t-Bu on pytrz. The LUMO of compounds **1–9** involves mostly the pytrz ligand, with a small contribution from the triazole ring of the ptrz ligand. The computational data along with the electrochemical data are listed in **Table 3**. Further details can be found in the SI.

TD-DFT calculations showed that the HOMO to LUMO transitions are dominant in the vertical excitation of S_0 to S_1 (>80%) and are the main component in S_0 to T_1 vertical excitation (>50%) for all Pt(II) compounds. The experimental and calculated HOMO and LUMO energies for compound **1–9** are shown in **Figure 13**. The calculated HOMO energies are in good agreement with the ones determined experimentally except for compound **5** and **6**, which is reasonable because it is known that TD-DFT produces substantial errors in predicting excitation energies that involve large charge-transfer contributions such as the case of **5** and **6**. The HOMO–LUMO energy gaps and the first triplet state energies are in general bigger for compounds bearing a CF_3 group, compared to those with a *t*-Bu group (i.e., **1** versus **2**, **3** versus **4**, and **8** versus **9**), except for compounds **5** and **6**, which could be attributed mainly to the destabilization effect of the t-Bu group and the stabilization effect of the CF_3 group on the HOMO energy level. Based on the TD-DFT data, the phosphorescence in all complexes except **5** and **6** may be attributed to transitions involving an admixture of ^{3}LC/MLCT states while that of **5** and **6** is mainly from CT transitions localized on the Ph_2N-phenyl unit and the pytrz chelate unit, which is consistent with the long phosphorescent decay lifetimes of **5** and **6**.

2.6. Electrophosphorescence

Based on their excellent phosphorescent quantum efficiency, their blue or blue-green emission colors and the least tendency of excimer formation, compounds **7–9** were chosen for electrophosphorescence evaluation. EL devices with various host and charge transport materials were fabricated for these

Table 3. Experimental HOMO–LUMO energy and TD-DFT data for compound 1–9.

	Experimental data				TD-DFT data					
	[a] E^{red}	HOMO[b] (eV)	LUMO[b] [eV]	[c] E_g (T_1)	HOMO [eV]	LUMO [eV]	H-L gap [eV]	[d] E_g (T_1)	% H → L (S_0→S_1)	f (S_0→S_1)
1	–2.39	–5.50	–2.41	2.62	–5.31	–1.39	3.92	2.69	93	0.0100
2	–2.50	–5.58	–2.30	2.82	–5.61	–1.66	3.95	2.88	90	0.0068
3	–2.50	–5.35	–2.30	2.66	–5.47	–1.55	3.92	2.71	95	0.0245
4	–2.34	–5.88	–2.46	2.82	–5.88	–1.80	4.08	2.91	91	0.0012
5	–2.43	–5.25	–2.37	2.51	–4.57	–1.39	3.18	2.54	98	0.0287
6	–2.32	–5.30	–2.48	2.48	–4.60	–1.61	2.99	2.42	99	0.0186
7	–2.30	–5.61	–2.50	2.77	–5.55	–1.66	3.89	2.87	81	0.0057
8	–2.29	–5.52	–2.51	2.70	–5.25	–1.36	3.89	2.69	93	0.0144
9	–2.24	–5.67	–2.56	2.77	–5.52	–1.61	3.91	2.88	83	0.0054

[a]Recorded in CH_3CN/THF with 0.10 M Bu_4NPF_6 at a scan rate of either 100 mV s^{-1} or 200 mV s^{-1} (vs Cp_2Fe/Cp_2Fe^+); [b]The LUMO energy was estimated using the reduction potential and the HOMO energy was calculated using the absorption edge and the LUMO energy; [c]The triplet energy value (T_1) was estimated using the emission spectra at 77 K; [d]S_0→T_1 vertical excitation energies.

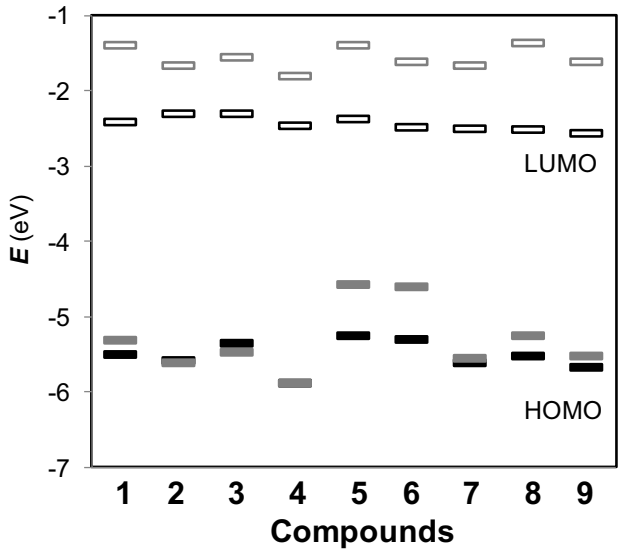

Figure 13. The experimental (black) and calculated (gray) HOMO and LUMO energies for compound **1**–**9**.

three compounds. The two typical device structures used in our investigation are **A**: ITO (70 nm)/MoO_3 (1 nm)/TAPC (60 nm)/POPCPA : x% Pt dopant (15 nm)/Tm3PyPb (40 nm)/LiF (1 nm)/Al (100 nm) and **B**: ITO (70 nm)/MoO_3 (1 nm)/TAPC (60 nm)/26mCPy : x% Pt dopant (15 nm)/Tm3PyPb (40 nm)/LiF (1 nm)/Al (100 nm). The electron transport material 1,3,5-tri(m-pyrid-3-yl-phenyl)benzene (Tm3PyPb) and the hole transport material 1,1-bis[(di-4-tolylamino)phenyl] cyclohexane (TAPC) were selected because of their high triplet energy. Likewise, the host material (4-{1-[4-(diphenylphosphoryl)phenyl]cyclohexyl} phenyl)-bis(4-methylphenyl) amine (POPCPA)[15b] and 2,6-bis(*N*-carbazolyl)pyridine (26mCPy)[15a] were selected because of their high triplet energy (2.93 eV and 2.80 eV, respectively) and their relatively high LUMO level which is higher than those of **7**–**9** (triplet energy ≈ 2.7 eV), which could be effective in facilitating the confinement of the triplet exciton from the Pt(II) compounds.[1c,15] Unfortunately, however, the EL devices for the CF_3-substituted compounds **7** and **9** were found to be dominated by either excimers of the Pt(II) compound or exciplexes formed likely between the dopant and the host molecule or the charge transport molecule with a low brightness and efficiency (see SI). This may be caused by the high triplet energy of compounds **7** and **9**, the poor match of the energy level with the host material, and their tendency to form excimers as indicated by the 77 K phosphorescent spectrum of **7**. A similar trend was observed previously in $BMes_2$-functionalized Pt-ptrz compounds with a CF_3 substituted pytrz ancillary ligand.[9e] For the *t*-Bu substituted compound **8**, greenish-blue EL spectra (λ_{max} = 475 nm) that match very well with the PL spectrum of **8** were obtained using both device structure **A** and **B** and the doping level of **8** up to 10% in the device. Nonetheless, the device **B** structure was found to be more efficient than **A** for compound **8** (EQE maximum = 11.7% at a 10% doping level). Therefore, the discussion will be focused on EL devices of compound **8** using the structure **B**. The details for other EL devices can be found in the SI. The device structure **B** and the structures of the materials used for compound **8** are shown in **Figure 14**. Three sets of devices with a doping level of 2%, 5%, and 10%, respectively, were examined and the data are shown in **Figure 15** and **Table 4**. The EL spectra remain the same as the doping concentration increased from 2% to 10%, producing a greenish blue color with λ = 477 nm and CIE (x,y) of (0.18, 0.42). The lack of excimer emission of the EL devices of **8** is in sharp contrast to EL devices of the borylated compound ($BMes_2$)-**7**,[9e] which displayed a distinct excimer peak at the 10% doping level using the same device structure **B**. This clearly demonstrates the effectiveness of introducing a bulky non-boryl group at the *para*-position of the ptrz ligand in reducing excimer emission while maintaining the blue-green EL emission color. The current efficiency, power efficiency and external quantum efficiency increase as the doping concentration increases, probably due to reduced triplet-triplet annihilation. The device with a 10% of **8** displays the peak current efficiency, the power efficiency and the external quantum efficiency of 40.1 cd/A, 39.4 lm/W and 16.7%, respectively, which are retained at 31.1 cd/A, 22.2 lm/W and 12.9%, respectively, at 100 cd/m^2. These preliminary results are very good for the new blue-green Pt(II) emitter compound. The performance of compound **8** can be certainly improved with optimized device structures.

Preliminary investigation for device **B** indicated that this device has a relatively poor stability with apparent decrease of emission brightness after the device was monitored for a few

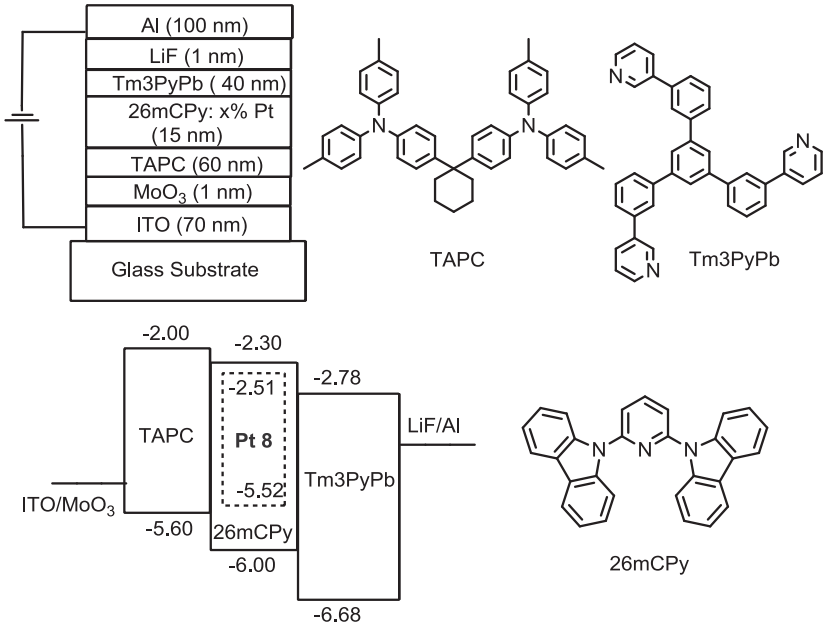

Figure 14. The structure and the materials for the EL devices (**B**) of compound **8**.

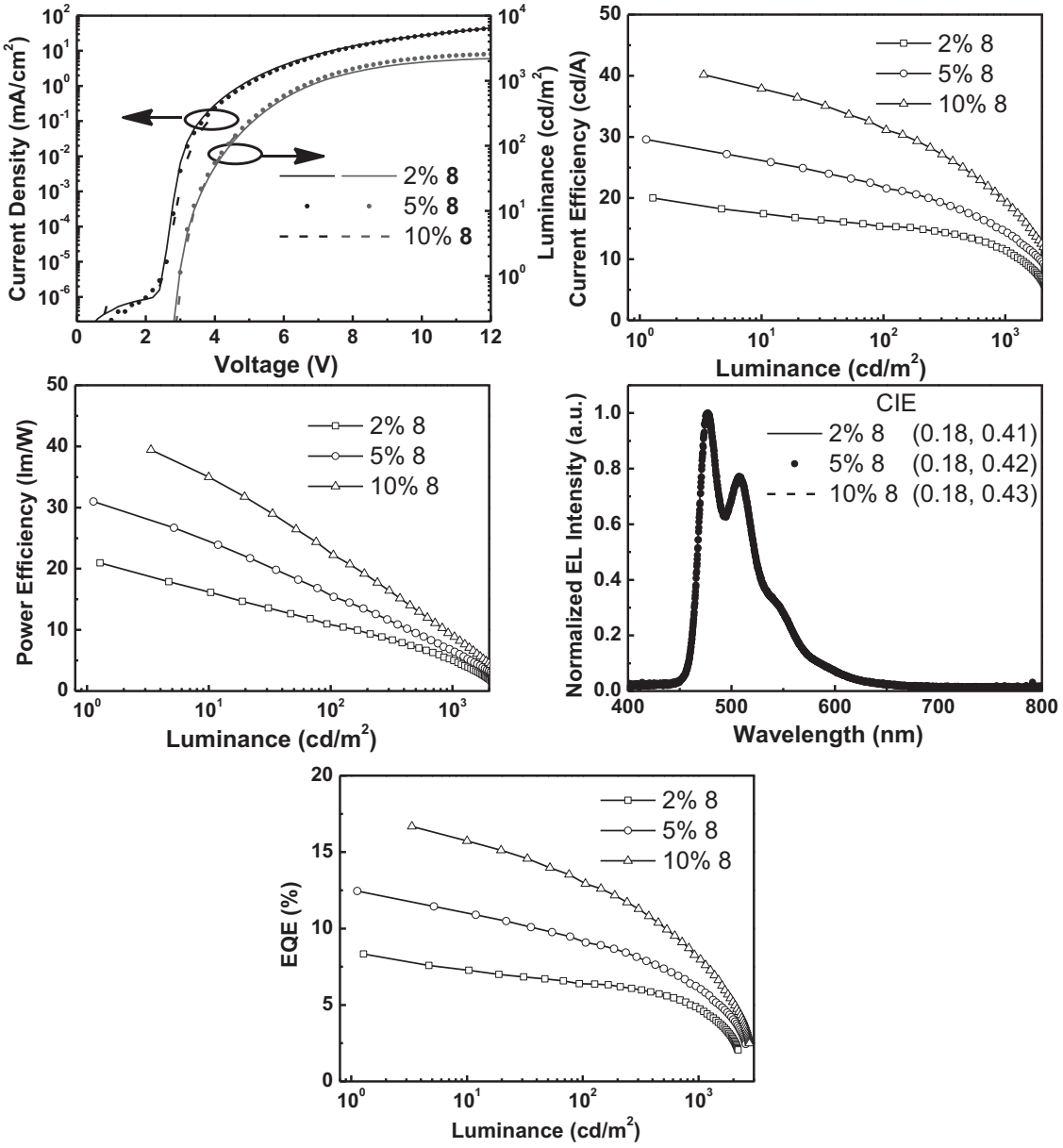

Figure 15. *L–J–V* and current efficiency, power efficiency, EL spectra and EQE–*L* diagrams of the EL devices based on **8**.

minutes.[17] This could be caused by the poor matching of the host material and the charge transport materials or the intrinsic poor stability of the triplet blue emitter due to its high exciton energy. Efforts are being taken to probe and understand the cause of the poor stability of device **B**, and to seek better host materials for the new triplet blue emitters. The details will be reported in due course.

3. Conclusions

New Pt(II) compounds based on a ptrz and a pytrz chelate core have been found to produce bright phosphorescence. The attachment of bulky substituents such as NPh_2 and CPh_3 at the *para*-position of the ptrz ligand was found to be highly effective in minimizing excimer emission and enhancing the phosphorescent quantum efficiency. Using this approach, green and blue phosphorescent Pt(II) compounds with near unity quantum efficiency have been achieved. Bluish-green EL devices based on one of the new Pt(II) emitters have been demonstrated to have external efficiencies comparable to those of the *meta*-$BMes_2$ substituted analogue, but with much less excimer or no excimer emission. Furthermore, the new non-borylated Pt(II) compounds was found to have a much higher thermal stability than the *meta*-$BMes_2$ substituted analogues. For the new deep blue emitters, better host and charge transport materials are necessary in order to fabricate blue EL devices that are excimer free, which will be investigated by our team.

Table 4. EL device data for **8**.

	EL λ_{max} [nm][a]		η_{ext} [%][d]				CIE		
Device		V_{on} [V][b]	L [cd/m^2, V][c]	10 cd/m^2	100 cd/m^2	1000 cd/m^2	η_c [cd/A][e]	η_p [lm/W][e]	(x,y)
2% **8**	476	3.0	2192, 12.0	7.3	6.4	4.8	20.0	21.0	(0.18, 0.41)
5% **8**	477	3.0	2559, 12.0	11.1	9.1	6.3	29.6	31.0	(0.18, 0.42)
10% **8**	477	3.0	2735, 12.0	15.9	12.9	8.0	40.1	39.4	(0.18, 0.43)

[a]Value taken at I = 20 mA. [b]The applied voltage (V_{on}) is defined as brightness of 1 cd/m^2; [c]The luminance (L) is the maximum value; [d]External quantum efficiency (EQE, η_{ext}); [e]Current efficiency (η_c) and power efficiency (η_p) are the maximum values.

4. Experimental Section

General Experimental Information: All Reactions were carried out under nitrogen atmosphere unless otherwise noted. Reagents were purchased from Aldrich chemical company and used as received. TLC and flash chromatography were performed on silica gel. ^{1}H and ^{13}C NMR spectra were recorded on Bruker Avance 300 and 400 MHz spectrometers. Deuterated solvents were purchased from Cambridge Isotopes and used without further purification. Excitation and emission spectra were obtained on a Photon Technology International QuantaMaster Model 2 spectrometer. Solid state quantum efficiency measurements were performed using the same spectrometer with an integration sphere. Phosphorescent decay lifetimes were measured with a Photon Technology International Phosphorescent lifetime spectrometer using a xenon flash lamp as the excitation source. Solution phosphorescence quantum yields of compounds **1**, **3–6** and **8** were measured relative to Ir(ppy)$_3$ in degassed dichloromethane (Φ = 0.95) at 298 K.[16] UV–Vis spectra were recorded on a Varian Carry 50 UV/Vis spectrophotometer. Cyclic voltammetry experiments were conducted on a BAS CV-50W analyzer with a scan rate of either 100 or 200 mV s^{-1}, using 0.1M NBu_4PF_6 in acetonitrile and THF solvent mixture as the supporting electrolyte. The electrochemical cell was a standard three-compartment cell composed a Pt working electrode, a Pt auxiliary electrode and an Ag/AgCl reference electrode. Ferrocene was used as the internal standard ($E^{1/2}$ = 0.55 V). Thermogravimetric analyses (TGA) were performed using a TA Q5000 instrument under nitrogen. The samples were heated to 100 °C at a speed of 10 °C/min. The temperature was maintained for 10 min before further heating to 480°C at 10°C/min. Elemental analyses were performed at the Elemental Analysis Laboratory, University of Montreal. TD-DFT calculations were carried out using the Gaussian 09 software at the High Performance Computing Virtual Laboratory (HPCVL) at Queen' s University. All computations were performed at the B3LYP level of theory[14] using LAN2LD as the basis set for Pt and 6–31G(d) for all other atoms. 1-Benzyl-4-phenyltriazole (**L1**) and 1-benzyl-4-(2,4-difluorophenyl)-1H-1,2,3-triazole (**L2**) are previously known molecules and were prepared according to the literature procedures.[10] *N,N*-diphenyl-4-(1-benzyl-1H-1,2,3-triazol-4-yl) aniline (**L3**), 1-benzyl-4-(4-tritylphenyl)- 1H-1,2,3-triazole (**L4**) and 1-benzhydryl-4-(4-tritylphenyl)-1H-1,2,3-triazole (**L5**) were prepared using procedures similar to the ones described previously by our group.[9e] The ancillary ligands *t*-bu-pytrz-Me and CF_3-pytrz-Me were synthesized according to literature procedures.[2d,11]

Synthesis of (4-ethynylphenyl)diphenylamine: A 100 mL three-neck round bottomed flask, equipped with a magnetic stir bar and a condenser, was charged with (4-bromophenyl)diphenylamine (1.0 g, 3.08 mmol), trimethylsilylacetylene (0.60 mL, 4.62 mmol), $Pd(PPh_3)Cl_2$ (0.11 g, 0.30 mmol), CuI (0.03 g, 0.15 mmol) and 40 mL of degassed THF/triethylamine (v:v = 3:1). The mixture was stirred at 80 °C for 20 hrs, concentrated under reduced pressure, dissolved in CH_2Cl_2 and washed sequentially with a saturated NH_4Cl solution, water and brine. The organic layer was dried over $MgSO_4$, filtered and the solvent was removed under reduced pressure. The solid was then purified using flash chromatography on silica using 4% ethyl acetate in hexane as the eluent. The resulting white solid was dissolved in 10 mL of THF and treated with NaOH in methanol (20 mL of a 2.0 M solution). After stirring for 2 hrs, the resulting mixture was concentrated under reduced pressure. After extraction with CH_2Cl_2, the organic layer was dried over $MgSO_4$, filtered and the solvent was removed under reduced pressure to give the product (4-ethynylphenyl)diphenylamine as a white solid (0.50 g, 60% Yield). ^{1}H NMR (300 MHz, $CDCl_3$, δ) 7.50–7.00 (m, 14H), 3.04 (s, 1H).

Synthesis of ((4-ethynylphenyl)methanetriyl)tribenzene: This molecule was prepared using the same procedure as for (4-ethynylphenyl) diphenylamine except replacing (4-bromophenyl)diphenyl amine with ((4-iodophenyl)methanetriyl)tribenzene (74% Yield). ^{1}H NMR (300 MHz, $CDCl_3$. δ) 7.40 (d, J = 8.5 Hz, 2H), 7.35–7.05 (m, 17H), 3.06 (s, 1H).

*Synthesis of N,N-diphenyl-4-(1-benzyl-1H-1,2,3-triazol-4-yl) aniline (***L3***)*: To a 50 mL Schlenk flask equipped with a magnetic stir bar was added (4-ethynylphenyl)diphenylamine (0.50 g, 1.86 mmol), benzyl azide (0.29 g, 2.21 mmol), diisopropylethylamine (0.475 g, 3.68 mmol), tris[(1-benzyl-1*H*-1,2,3-triazol-4-yl)-methyl]amine (1 mol%) and 30 mL of CH_2Cl_2. The resulting solution was bubbled with nitrogen gas for 20 minutes. $[Cu(CH_3CN)_4]PF_6$ (1 mol%) was added as a catalyst. After the resulting mixture was stirred overnight, the solvent was removed under reduced pressure. The crude product was re-dissolved in CH_2Cl_2 and washed with saturated NH_4Cl solution, water and brine. The organic layer was dried over $MgSO_4$, filtered and the solvent was removed under reduced pressure. The product was then purified using flash chromatography on silica (1:1 hexanes:ethyl acetate as the eluent) to afford 0.54 g of *N,N*-diphenyl-4-(1-benzyl-1H- 1,2,3-triazol-4-yl) aniline as a white solid (72% yield). ^{1}H NMR (300 MHz, $CDCl_3$, δ) 7.68 (d, J = 8.8 Hz, 2H), 7.60 (s, 1H), 7.45–7.36 (m, 3H), 7.35–7.20 (m, 6H), 7.19–6.98 (m, 8H), 5.59 (s, 2H).

*Synthesis of 1-benzyl-4-(4-tritylphenyl)-1H-1,2,3-triazole (***L4***)*: This compound was prepared using the same procedure as for **L3** except replacing (4-ethynylphenyl)diphenylamine with ((4-ethynylphenyl) -methanetriyl)tribenzene (62% Yield). ^{1}H NMR (300 MHz, $CDCl_3$, δ) 7.79 (d, J = 8.3 Hz, 2H), 7.63 (s, 1H), 7.45–7.10 (m, 22H), 5.59 (s, 2H).

*Synthesis of 1-benzhydryl-4-(4-tritylphenyl)-1H-1,2,3-triazole (***L5***)*: This compound was prepared using the same procedure as that for **L3** except replacing (4-ethynylphenyl)diphenylamine and benzyl azide with ((4-ethynylphenyl)methanetriyl)tribenzene and (azidomethylene) dibenzene, respectively (71% Yield). ^{1}H NMR (300 MHz, $CDCl_3$, δ) 7.71 (d, J = 8.0 Hz, 2H), 7.59 (s, 1H), 7.45–7.10 (m, 28H).

General Procedure for the Synthesis of Pt(II) Compounds: The ligand (0.20 mmol) and $[PtMe_2(SMe_2)]_2$ (0.11 mmol) were added to a 20 mL vial with a screw cap containing 5 mL of acetone. The mixture was heated at 70 °C for 1 h before 1 mL of 0.1 M solution of TsOH in THF was added. The resulting solution was stirred for 1 h, then 0.22 mmol of the corresponding pytrz ligand in acetone was added and the mixture was stirred at ambient temperature for 2 days. After the solvent was removed under reduced pressure, the product was extracted with CH_2Cl_2, and washed with water and brine. The combined organic phase was dried over $MgSO_4$, filtered and purified on a silica column. ^{13}C NMR spectra were not recorded for all Pt(II) compounds because of their poor solubility. The Pt(II) compounds have the tendency to co-crystallize with solvent molecules such as THF and CH_2Cl_2. For some of the compounds, the solvent molecules were positively identified in their

crystal lattices. For elemental analysis, all samples were dried under vacuum at ambient temperature. Nonetheless, many of the compounds still show solvent molecules trapped inside the crystal lattice.

(L1)Pt(t-Bu) (**1**): Yield 23%. ^{1}H NMR (300 MHz, CD_2Cl_2, δ) 9.35 (d, J = 4.9 Hz, 1H), 9.00 (d, J = 7.7 Hz, 1H), 7.81 (s, 1H), 7.49–7.26 (m, 6H), 7.25–6.95 (m, 4H), 5.49 (s, 2H), 2.41 (s, 3H), 1.40 (s, 9H). Anal. calcd for **1** ($C_{27}H_{27}N_7Pt$): C 50.07, H 4.12 N 14.99; found: C 50.31, H 4.22, N 15.21.

(L1)Pt(CF_3) (**2**): Yield 17%. ^{1}H NMR (400 MHz, CD_2Cl_2, δ) 9.32 (d, J = 5.6 Hz, 1H), 8.69 (d, J = 7.6 Hz, 1H), 7.79 (s, 1H), 7.45–7.29 (m, 6H), 7.18 (d, J = 5.6 Hz, 1H), 7.14 (dd, J = 7.3 Hz, 1.3 Hz, 1H), 7.08 (td, J = 7.5 Hz, 1.5 Hz, 1H), 7.01 (td, J = 7.3 Hz, 1.1 Hz, 1H), 5.51 (s, 2H), 2.41 (s, 3H). Anal. calcd for **2**·1/2THF ($C_{26}H_{22}F_3N_7O_{0.5}Pt$): C 45.09, H 3.20, N 14.16; found: C 44.84, H 2.70, N 14.30.

(L2)Pt(t-Bu) (**3**): Yield 39%. ^{1}H NMR (400 MHz, CD_2Cl_2, δ) 9.26 (d, J = 5.8 Hz, 1H), 8.66 (dd, J = 10.2 Hz, 2.4 Hz, 1H), 7.77 (s, 1H), 7.47 (d, J = 1.1 Hz, 1H), 7.41–7.30 (m, 5H), 7.10 (dd, J = 5.6 Hz, 1.3 Hz, 1H), 6.51 (ddd, J = 10.0 Hz, 9.0 Hz, 2.4 Hz, 1H), 5.51 (s, 2H), 2.42 (s, 3H), 1.40 (s, 9H). Anal. calcd for **3**·1THF ($C_{31}H_{33}F_2N_7OPt$): C 49.46, H 4.42, N 13.03; found: C 49.38, H 4.24, N 13.37.

(L2)Pt(CF_3) (**4**): Yield 46%. ^{1}H NMR (400 MHz, THF-d_8, δ) 9.44 (d, J = 5.7 Hz, 1H), 8.52 (dd, J = 9.9 Hz, 2.3 Hz, 1H), 8.15 (s, 1H), 7.95 (s, 1H), 7.55–7.30 (m, 6H), 6.66 (m, 1H), 5.76 (s, 2H), 2.53 (s, 3H). HRMS (ESI) for $C_{24}H_{17}N_7F_5Pt$ $[M+H]^+$: calcd. 693.1113, found 693.1132; $[M_2]^+$: 1384.2066, found 1384.2135. Anal. calcd for **4** ($C_{24}H_{16}F_5N_7Pt$): C 41.63, H 2.33, N 14.16; found: C 41.86, H 2.16, N 13.64.

(L3)Pt(t-Bu) (**5**): Yield 20%. ^{1}H NMR (300 MHz, CD_2Cl_2, δ) 9.39 (d, J = 5.9 Hz, 1H), 8.85 (s, 1H), 7.78 (s, 1H), 7.51–7.26 (m, 6H), 7.25–6.98 (m, 10H), 6.90 (t, J = 7.2 Hz, 2H), 6.70 (d, J = 8.2 Hz, 1H), 5.51 (s, 2H), 2.40 (s, 3H), 1.06 (s, 9H). Anal. calcd for **5** ($C_{39}H_{36}N_8Pt$): C 57.70, H 4.47, N 13.80; found: C 57.27, H 4.31, N 13.45.

(L3)Pt(CF_3) (**6**): Yield 14%. ^{1}H NMR (400 MHz, CD_2Cl_2, δ) 9.42 (d, J = 5.6 Hz, 1H), 8.51 (d, J = 2.3 Hz, 1H), 7.84 (s, 1H), 7.40 (s, 1H), 7.39–7.31 (m, 5H), 7.27–7.14 (m, 5H), 7.12–7.01 (m, 5H), 6.96 (t, J = 7.3 Hz, 2H), 6.75 (dd, J = 8.2 Hz, 2.1 Hz, 1H), 5.51 (s, 2H), 2.41 (s, 3H). Anal. calcd for **6**·1hexane ($C_{42}H_{41}F_3N_8Pt$): C 55.44, H 4.54, N 12.31; found: C 54.89, H 4.23, N 12.29.

(L4)Pt(CF_3) (**7**): Yield 24%. ^{1}H NMR (400 MHz, CD_2Cl_2, δ) 9.38 (d, J = 5.8 Hz, 1H), 8.87 (d, J = 1.8 Hz, 1H), 7.86 (s, 1H), 7.45–6.95 (m, 24H), 5.46 (s, 2H), 2.41 (s, 3H). Anal. calcd for **9**·1THF ($C_{47}H_{40}F_3N_7OPt$): C 58.14, H 4.15, N 10.10; found: C 58.39, H 4.18, N 10.39.

(L5)Pt(t-Bu) (**8**): Yield 22%. ^{1}H NMR (400 MHz, CD_2Cl_2, δ) 9.12 (d, J = 5.6 Hz, 1H), 9.07 (d, J = 1.8 Hz, 1H), 7.72 (s, 1H), 7.49 (s, 1H), 7.45–7.00 (m, 28H), 6.98 (d, J = 4.5 Hz, 1H), 2.35 (s, 1H), 1.03 (s, 9H). Anal. calcd for **8** ($C_{49}H_{36}N_7Pt$): C 64.85, H 4.71, N 10.18; found: C 65.11, H 4.64, N 10.09.

(L5)Pt(CF_3) (**9**): Yield 20%. ^{1}H NMR (400 MHz, CD_2Cl_2, δ) 9.16 (d, J = 5.6 Hz, 1H), 8.87 (d, J = 1.5 Hz, 1H), 7.83 (s, 1H), 7.51 (s, 1H), 7.45–6.95 (m, 29H), 2.38 (s, 3H). Anal. calcd for **9**·1THF ($C_{53}H_{44}F_3N_7OPt$): C 60.80, H 4.24, N 9.36; found: C 60.96, H 3.87, N 9.34.

EL Device Fabrication: The hole-injection material MoO_3 and electron-injection material LiF were purchased from Sigma-Aldrich and used as received. The hole-transporting material TAPC and electron-transporting material Tm3PyPB were purchased from Luminescence Technology Corporation and purified by train sublimation prior to deposition. The host materials POPCPA and 26mCPy were synthesized according to the literature procedures[15] Devices were fabricated in a three-chamber evaporator (EL-OEL cluster tool) with a base pressure of $\approx 1 \times 10^{-7}$ Pa without breaking vacuum. The ITO anode is commercially patterned and coated on glass substrates 50 mm × 50 mm with a sheet resistance less than 15 Ω. Substrates were ultrasonically cleaned with a standard regiment of Alconox®, acetone, and methanol followed by UV ozone treatment for 15 min. The active area for all devices was 2 mm^2. The film thicknesses were monitored by a calibrated quartz crystal microbalance and were further verified for single-carrier devices using capacitance-voltage measurements (Agilent 4294A). I-V characteristics were measured using a HP4140B picoammeter in ambient air. Luminance measurements and EL spectra were taken using a Minolta LS-110 luminance meter and an Ocean Optics USB200 spectrometer with bare fiber, respectively. The external quantum efficiency of EL devices was calculated following the standard procedure.[18]

X-Ray Crystallography Analysis: Single crystals of **4**, **5**, **7**–**9** were obtained from either CH_2Cl_2 or THF by slow evaporation of the solvent. For some of the compounds, it was necessary to add either methanol or hexanes to facilitate the crystal growth. The crystals were mounted on glass fibers and the data were collected on a Bruker Apex II single-crystal X-ray diffractometer with graphite-monochromated M_o Kα radiation, operating at 50 kV and 30 mA, and at 180 K. Data were processed on a PC with the aid of the Bruker SHELXTL software package (version 6.14) and corrected for absorption effects.[19] All structures were solved using direct methods. The crystals of **4** and **8** belong to the triclinic space group P-1, those of **7** and **9** belong to the monoclinic space group $P2_1/n$, while **5** belongs to the monoclinic space group C2/c. CH_2Cl_2 solvent molecules were located in the lattices of **8** (two CH_2Cl_2 per molecule of **8**) and **9** (2.4 CH_2Cl_2 per molecule of **9**) and refined successfully. THF solvent molecules were found in the lattice of **7** (1 THF per molecule of **7**) and refined successfully. All non-hydrogen atoms were refined anisotropically. Complete crystal structural data can be found in the Supporting Information. [CCDC No. 1013543 (**4**), 1013542 (**5**), 1013541 (**7**), 1013539 (**8**), and 1013540 (**9**) contain the supplementary crystallographic data for this paper.[20]

Supporting Information

Supporting Information is available from the Wiley Online Library or from the author.

Acknowledgements

The authors thank the Natural Sciences and Engineering Research Council of Canada for financial support. S.W. thanks the Canada Council for the Arts for the Killam Research Fellowship. The authors are grateful to Mr. Yu Wang and Prof. Guo-Jun Liu for their assistance in recording the TGA diagrams.

Received: July 16, 2014
Revised: August 13, 2014
Published online: September 18, 2014

[1] a) H. Fu, Y.-M. Cheng, P.-T. Chou, Y. Chi, *Mater. Today* **2011**, *14*, 472; b) Y.-S. Tyan, *J. Photonics Energy* **2011**, *1*, 011009; c) K. S. Yook, J. Y. Lee, *Adv. Mater.* **2012**, *24*, 3169; d) C.-L. Ho, W.-Y. Wong, *New J. Chem.* **2013**, *37*, 1665.

[2] a) K. Dedeian, J. Shi, N. Shepherd, E. Forsythe, D. C. Morton, *Inorg. Chem.* **2005**, *44*, 4445; b) J. Li, P. I. Djurovich, B. D. Alleyne, M. Yousufuddin, N. N. Ho, J. C. Thomas, J. C. Peters, R. Bau, M. E. Thompson, *Inorg. Chem.* **2005**, *44*, 1713; c) S.-C. Lo, C. P. Shipley, R. N. Bera, R. E. Harding, A. R. Cowley, P. L. Burn, I. D. W. Samuel, *Chem. Mater.* **2006**, *18*, 5119; d) E. Orselli, G. S. Kottas, A. E. Konradsson, P. Coppo, R. Fröhlich, L. De Cola, A. van Dijken, M. Büchel, H. Börner, *Inorg. Chem.* **2007**, *46*, 11082; e) C.-F. Chang, Y.-M. Cheng, Y. Chi, Y.-C. Chiu, C.-C. Lin, G.-H. Lee, P.-T. Chou, C.-C. Chen, C.-H. Chang, C.-C. Wu, *Angew. Chem. Int. Ed.* **2008**, *47*, 4542; f) Y.-C. Chiu, Y. Chi, J.-Y. Hung, Y.-M. Cheng, Y.-C. Yu, M.-W. Chung, G.-H. Lee, P.-T. Chou, C.-C. Chen, C.-C. Wu, H.-Y. Hsieh, *ACS Appl. Mater. Interfaces.s* **2009**, *1*, 433; g) Y. You, S. Y. Park, *Dalton Trans.* **2009**, 1267; h) T. Peng, Y. Yang, Y. Liu, D. Ma, Z. Hou, Y. Wang, *Chem. Commun.* **2011**, *47*, 3150; i) Y. Kang, Y.-L. Chang, J.-S. Lu, S.-B. Ko, Y. Rao, M. Varlan, Z.-H. Lu, S. Wang, *J. Mater. Chem. C* **2013**, *1*, 441.

[3] a) M.-S. Lin, S.-J. Yang, H.-W. Chang, Y.-H. Huang, Y.-T. Tsai, C.-C. Wu, S.-H. Chou, E. Mondal, K.-T. Wong, *J. Mater. Chem.* **2012**, *22*, 16114; b) C. W. Lee, J. Y. Lee, *Adv. Mater.* **2013**, *25*, 5450; c) S. Lee, S.-O. Kim, H. Shin, H.-J. Yun, K. Yang, S.-K. Kwon, J.-J. Kim, Y.-H. Kim, *J. Am. Chem. Soc.* **2013**, *135*, 14321; d) M. Kim, J. Y. Lee, *Adv. Funct. Mater.* **2014**, *24*, 4164; e) H. Ye, D. Chen, M. Liu, S.-J. Su, Y.-F. Wang, C.-C. Lo, A. Lien, J. Kido, *Adv. Funct. Mater.* **2014**, *24*, 3268.

[4] a) J. Brooks, Y. Babayan, S. Lamansky, P. I. Djurovich, I. Tsyba, R. Bau, M. E. Thompson, *Inorg. Chem.* **2002**, *41*, 3055; b) R. C. Evans, P. Douglas, C. J. Winscom, *Coord. Chem. Rev.* **2006**, *250*, 2093; c) S. Develay, O. Blackburn, A. L. Thompson, J. A. G. Williams, *Inorg. Chem.* **2008**, *47*, 11129; d) J. Garethwilliams, S. Develay, D. Rochester, L. Murphy, *Coord. Chem. Rev.* **2008**, *252*, 2596; e) U. S. Bhansali, E. Polikarpov, J. S. Swensen, W.-H. Chen, H. Jia, D. J. Gaspar, B. E. Gnade, A. B. Padmaperuma, M. A. Omary, *Appl. Phys. Lett.* **2009**, *95*, 233304; f) J. Kalinowski, V. Fattori, M. Cocchi, J. A. G. Williams, *Coord. Chem. Rev.* **2011**, *255*, 2401; g) X. Yang, C. Yao, G. Zhou, *Platinum Metals Rev.* **2013**, *57*, 2.

[5] a) X. Yang, Z. Wang, S. Madakuni, J. Li, G. E. Jabbour, *Adv. Mater.* **2008**, *20*, 2405; b) L. Murphy, P. Brulatti, V. Fattori, M. Cocchi, J. A. G. Williams, *Chem. Commun.* **2012**, *48*, 5817; c) X.-C. Hang, T. Fleetham, E. Turner, J. Brooks, J. Li, *Angew. Chem. Int. Ed.* **2013**, *52*, 6753.

[6] H. L. Schläfer, G. Gliemann, *Basic principles of ligand field theory*, Wiley, New York **1969**.

[7] B. D' Andrade, S. R. Forrest, *Chem. Phys.* **2003**, *286*, 321.

[8] a) S. J. Farley, D. L. Rochester, A. L. Thompson, J. A. K. Howard, J. A. G. Williams, *Inorg. Chem.* **2005**, *44*, 9690; b) M. Cocchi, D. Virgili, V. Fattori, D. L. Rochester, J. A. G. Williams, *Adv. Funct. Mater.* **2007**, *17*, 285; c) J. D. Froehlich, R. Young, T. Nakamura, Y. Ohmori, S. Li, A. Mochizuki, M. Lauters, G. E. Jabbour, *Chem. Mater.* **2007**, *19*, 4991; d) Z. M. Hudson, C. Sun, M. G. Helander, H. Amarne, Z.-H. Lu, S. Wang, *Adv. Funct. Mater.* **2010**, *20*, 3426; e) C.-H. Chen, F.-I. Wu, Y.-Y. Tsai, C.-H. Cheng, *Adv. Funct. Mater.* **2011**, *21*, 3150; f) J. Kavitha, S.-Y. Chang, Y. Chi, J.-K. Yu, Y.-H. Hu, P.-T. Chou, S.-M. Peng, G.-H. Lee, Y.-T. Tao, C.-H. Chien, A. J. Carty, *Adv. Funct. Mater.* **2005**, *15*, 223; g) G. Zhou, Q. i. Wang, X. Wang, C.-L. Ho, W.-Y. Wong, D. Ma, L. Wang, Z. Lin, *J. Mater. Chem.* **2010**, *20*, 7472.

[9] a) Z. M. Hudson, M. G. Helander, Z.-H. Lu, S. Wang, *Chem. Commun.* **2011**, *47*, 755; b) Z. B. Wang, M. G. Helander, Z. M. Hudson, J. Qiu, S. Wang, Z. H. Lu, *Appl. Phys. Lett.* **2011**, *98*, 213301; c) Z. M. Hudson, C. Sun, M. G. Helander, Y.-L. Chang, Z.-H. Lu, S. Wang, *J. Am. Chem. Soc.* **2012**, *134*, 13930; d) Y.-L. Rao, D. Schoenmakers, Y.-L. Chang, J.-S. Lu, Z.-H. Lu, Y. Kang, S. Wang, *Chem. Eur. J.* **2012**, *18*, 11306; e) X. Wang, Y.-L. Chang, J.-S. Lu, T. Zhang, Z.-H. Lu, S. Wang, *Adv. Funct. Mater.* **2014**, *24*, 1911.

[10] C. Zhang, B. Huang, Y. Chen, D.-M. Cui, *New J. Chem.* **2013**, *37*, 2606.

[11] H. J. Park, J. N. Kim, H.-J. Yoo, K.-R. Wee, S. O. Kang, D. W. Cho, U. C. Yoon, *J. Org. Chem.* **2013**, *78*, 805.

[12] Z. M. Hudson, B. A. Blight, S. Wang, *Org. Lett.* **2012**, *14*, 1700.

[13] a) S. C. F. Kui, S. S.-Y. Chui, C.-M. Che, N. Zhu, *J. Am. Chem. Soc.* **2006**, *128*, 8297; b) T. J. Wadas, Q.-M. Wang, Y. Kim, C. Flaschenreim, T. N. Blanton, R. Eisenberg, *J. Am. Chem. Soc.* **2004**, *126*, 16841.

[14] M. J. Frisch, G. W. Trucks, H. B. Schlegel, G. E. Scuseria, M. A. Robb, J. R. Cheeseman, G. Scalmani, V. Barone, B. Mennucci, G. A. Petersson, H. Nakatsuji, M. Caricato, X. Li, H. P. Hratchian, A. F. Izmaylov, J. Bloino, G. Zheng, J. L. Sonnenberg, M. Hada, M. Ehara, K. Toyota, R. Fukuda, J. Hasegawa, M. Ishida, T. Nakajima, Y. Honda, O. Kitao, H. Nakai, T. Vreven, J. A. Montgomery Jr., J. E. Peralta, F. Ogliaro, M. J. Bearpark, J. Heyd, E. N. Brothers, K. N. Kudin, V. N. Staroverov, R. Kobayashi, J. Normand, K. Raghavachari, A. P. Rendell, J. C. Burant, S. S. Iyengar, J. Tomasi, M. Cossi, N. Rega, N. J. Millam, M. Klene, J. E. Knox, J. B. Cross, V. Bakken, C. Adamo, J. Jaramillo, R. Gomperts, R. E. Stratmann, O. Yazyev, A. J. Austin, R. Cammi, C. Pomelli, J. W. Ochterski, R. L. Martin, K. Morokuma, V. G. Zakrzewski, G. A. Voth, P. Salvador, J. J. Dannenberg, S. Dapprich, A. D. Daniels, Ö. Farkas, J. B. Foresman, J. V. Ortiz, J. Cioslowski, D. J. Fox, in *Gaussian 09, Vol*. Gaussian, Inc., Wallingford, CT, USA, **2009**.

[15] a) L. Xiao, Z. Chen, B. Qu, J. Luo, S. Kong, Q. Gong, J. Kido, *Adv. Mater.* **2011**, *23*, 926; b) S. Gong, Y.-L. Chang, K. Wu, R. White, Z.-H. Lu, D. Song, C. Yang, *Chem. Mater.* **2014**, *26*, 1463.

[16] T. Sajoto, P. I. Djurovich, A. B. Tamayo, J. Oxgaard, W. A. Goddard III, M. E. Thompson, *J. Am. Chem. Soc.* **2009**, *131*, 9813–9822.

[17] Q. Wang, H. Z. Sibnoi, X. Wang, S. Wang, H. Aziz, unpublished work.

[18] S. R. Forrest, D. D. C. Bradley, M. E. Thompson, *Adv. Mater.* **2003**, *15*, 1043.

[19] SHELXTL Version 6.14, Bruker Analytical X-ray Systems, copyright 2000–2003.

[20] These data can be obtained free of charge from The Cambridge Crystallographic Data Center via www.ccdc.cam.ac.uk/data_request/cif.